American Mineralogist, Volume 76, pages 1442–1445, 1991

LETTER

Imaging molecular-scale structure and microtopography of hematite with the atomic force microscope

PATRICIA A. JOHNSSON, CARRICK M. EGGLESTON
Department of Applied Earth Sciences, Stanford University, Stanford, California 94305, U.S.A.
MICHAEL F. HOCHELLA, JR.
Department of Geology, Stanford University, Stanford, California 94305, U.S.A.

ABSTRACT

The atomic force microscope (AFM) was used to image {001} surface microtopography and molecular-scale structure of two natural specular hematite samples. Topographic images in air and under H_2O showed that although the surface is atomically flat in some areas, pits and steps are abundant. Molecular-scale resolution in air showed a hexagonal array of peaks with ~5-Å spacing, representing surface Fe atoms with coordinated sorbates. Comparison with scanning-tunneling microscope (STM) images of the {001} surface-Fe-atom array in air, which also had hexagonal symmetry and ~5-Å spacing, showed that the scanning probe microscopes can produce similar high-resolution images of hematite even though they rely on different physical operating mechanisms. Results of these studies indicate that for conducting or semiconducting minerals, a combination of scanning-tunneling and atomic-force microscopy permits direct, in situ analysis of mineral surface structure and microtopography.

INTRODUCTION

As part of a study of mineral surface structure and reactivity, we used the recently developed atomic force microscope (AFM) to image the nanometer-scale microtopography and molecular-scale structure of the {001} surface of two natural specular hematite samples. We have chosen to study hematite not only because of its importance as a common accessory mineral in soils and aquifers but also because hematite is a semiconductor that has been studied by scanning-tunneling microscopy (STM) and low-energy electron diffraction (LEED) in our laboratory (Hochella et al., 1989; Eggleston et al., 1990). Hematite thus affords an excellent opportunity to compare AFM and STM images of subsamples from the same mineral specimens. Such a comparison is important because these two scanning probe microscopes rely on different physical operating mechanisms to produce high-resolution images of surfaces.

STM relies on detection of an electrical tunneling current to image microtopography and atomic-scale structure of conducting and semiconducting surfaces. STM has been applied successfully to the minerals hematite, pyrite, and galena (Hochella et al., 1989; Eggleston and Hochella, 1990; Sharp et al., 1990). Additionally, STM can provide spectroscopic information (Hochella, 1990); Eggleston et al. (1990, and unpublished data) have demonstrated that variation of sample bias voltage allows for selective imaging of the Fe and O arrays on hematite.

AFM does not rely on a tunneling current and thus extends the high-resolution capability to insulating surfaces. The AFM used here monitors the repulsive contact forces between an extremely sharp tip and a sample surface. Since its development, AFM has been used to image nanometer-scale morphology on albite (Hochella et al., 1990); molecular-scale structure of illite, montmorillonite, and several zeolites (Hartman et al., 1990; Weisenhorn et al., 1990); and atomic-scale structure of graphite (Binnig et al., 1986; Albrecht and Quate, 1988) and sodium chloride (Meyer and Amer, 1990). As shown here, AFM is particularly well suited to investigations in aqueous media.

EXPERIMENTAL

Samples and imaging

Two Brazilian specular hematite (α-Fe_2O_3) specimens from the Stanford Mineral Collection were used in this study. The hematite specimens displayed well-developed {001} parting and could be fractured to produce mirror-flat surfaces prior to imaging. No other preparation was necessary.

The AFM used in this study (Digital Instruments model AFM-1) is described by Hochella et al. (1990). Briefly,

0003–004X/91/0708–1442$02.00

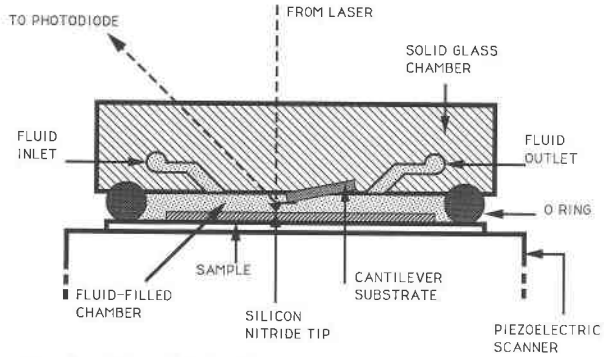

Fig. 1. Glass fluid cell used to image samples under deionized H_2O.

the AFM works by rastering a sample mounted on a piezoelectric tube under a sharp tip that is attached to or part of a cantilever. Deflection of the cantilever as the sample is moved under it is monitored via an "optical lever" consisting of laser light reflected off the end of the cantilever toward a photodiode. All images shown in this paper were obtained in the constant force mode, in which a feedback loop is used to adjust the height of the sample to keep the cantilever deflection constant during sample rastering. Estimated tracking forces were no greater than 10^{-7} N in air and may range as low as 10^{-9} N under H_2O. We used one-piece silicon nitride cantilever and tips from Park Scientific. The molecular- to atomic-scale STM and AFM images presented here were Fourier filtered to remove high-frequency noise and streaks; general peak shape and spacing were unaffected by this filtering process.

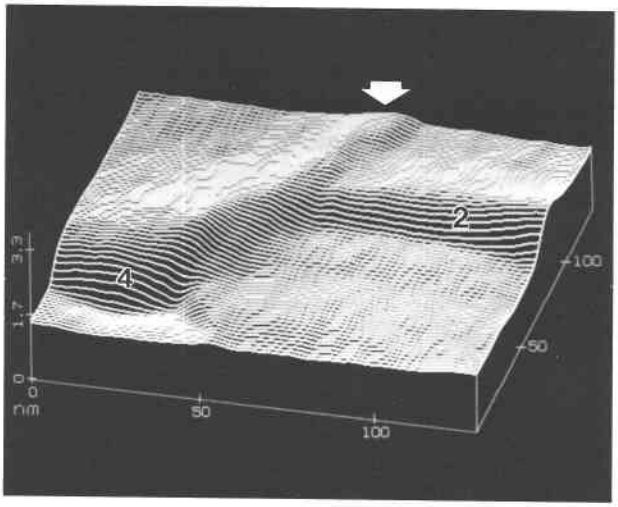

Fig. 2. AFM image of hematite {001} surface under deionized H_2O showing a complex set of terraces separated by 2- and 4-Å high steps; numbers refer to step heights. A fine crack or buckle present along one terrace is delineated with an arrow; this feature is not a step as terraces on either side have the same height. The line plot image display mode used here is excellent for showing topographic features but is otherwise equivalent to the top view images shown in Figures 3 and 4. Scale in nanometers (1 nm = 10 Å).

Fig. 3. Closeup along the edge of a small pit imaged in H_2O. This pit probably resulted from a fluid inclusion. In top view images such as this, darker tones represent increasing depth; maximum pit depth in image = 15 Å. Maximum relief along bottom of pit = 7 Å. Image dimensions = 210 × 210 nm.

Samples were imaged under deionized H_2O using a Digital Instruments glass cell that fits over the sample with an O-ring seal (Fig. 1). In this cell, the cantilever is completely immersed in fluid. Although separate inlet and outlet tubes allow for imaging under flowing conditions, the images shown here were produced under static fluid conditions.

Results and discussion

Nanometer-scale microtopography

In air and under H_2O, AFM images demonstrate that although the hematite surfaces are atomically flat in some areas, surface microtopography can be quite complex. Figure 2, an image obtained under H_2O, includes atomically flat terraces separated by 2- to 4-Å high steps. The step heights are measured from the centers of the terraces. The thickness of a single O layer in hematite is 2.3 Å; therefore, these steps are only one to two O atomic layers high. The steps probably are fracture features. Along with the steps, there are also linear features that may be fine cracks or buckles on the terraces; one such feature is depicted with an arrow in Figure 2.

Figure 3 shows the edge of a small pit imaged in H_2O. Maximum depth of the pit measured in cross section was found to be 15 Å; the relief along the bottom of the pit was at most 7 Å. The interior structure is reminiscent of botryoidal forms of hematite. This pit probably resulted from fluid captured during crystal growth, i.e., a fluid inclusion. However, we cannot rule out the possibility of dissolution by fluids migrating along microcracks.

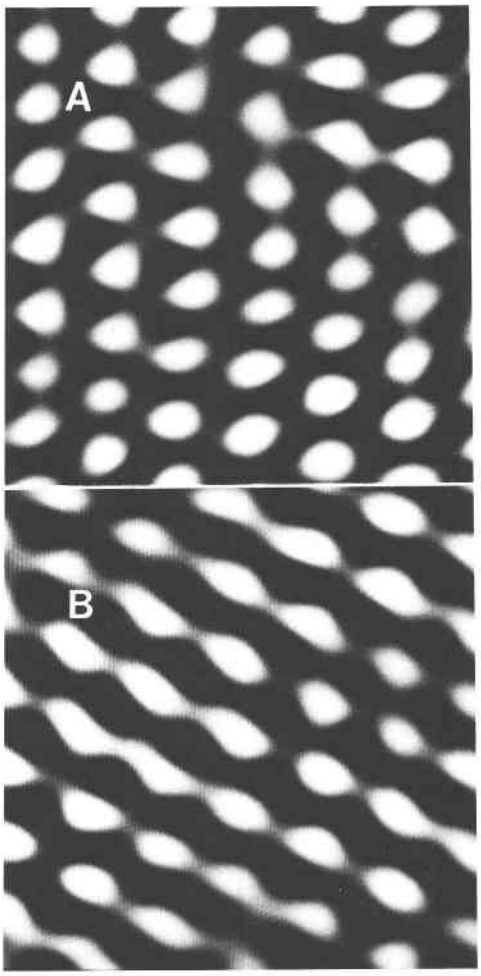

Fig. 4. Comparison of high-resolution AFM image of the hematite {001} surface under air (**A**) with an STM image at +1100 mV sample bias showing the surface-Fe-atom array (**B**). Peak spacing in both images is ~5 Å. Peak heights in **A** are ~1.0–1.5 Å; peak heights in **B** are ~0.2–0.3 Å. The peaks in the AFM image **A** represent surface Fe atoms with coordinated (O, OH, H_2O) sorbates. Sample drift causes the slight waviness in the AFM image **A**; the diagonal connections between the peaks in the STM image **B** are a scanning artifact. Image dimensions for **A** and **B** = 3 × 3 nm.

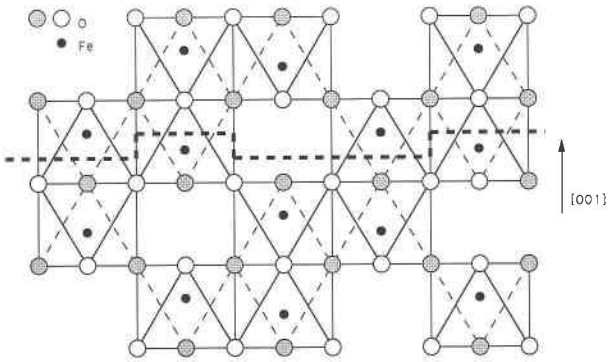

Fig. 5. Schematic of hematite crystal structure perpendicular to the {001} surface in the (110) plane. Dashed line delineates suspected trace of fracture parallel to {001}. The displaced positions of the Fe atoms within their octahedra have been exaggerated for clarity. O atoms depicted by open symbols lie above the Fe plane; stippled O atoms are below. Note that equivalent Fe atoms in this projection repeat every 8.7 Å rather than every 5 Å as in the (100) projection on the {001} surface.

Molecular-scale surface structure

Figure 4A shows the molecular-scale surface structure of the hematite {001} surface imaged by AFM in air. In this figure, a hexagonal array of peaks (light areas) with ~5-Å nearest neighbor spacing is apparent. Peak heights are ~1.0 to 1.5 Å. This image can be interpreted by consideration of the known hematite structure and by comparison with LEED and STM analyses of hematite surface structure.

The bulk structure of hematite consists of a closest-packed array of O atoms with two out of three octahedral sites filled with Fe atoms. The hexagonal unit cell has a = 5.04 Å and contains pairs of Fe-centered octahedra distributed in an hexagonal fashion around a vacancy. One member of each Fe pair shares a face with an Fe-centered octahedron in the next layer down; the other is over a vacancy (Fig. 5). Thus, the octahedra are somewhat distorted by the local atomic attractive and repulsive forces associated with shared and unshared Fe polyhedral faces and edges (Blake et al., 1966). In the direction perpendicular to (001), this distortion is manifested in different Fe-O bond lengths to the overlying and underlying O layers. As depicted in Figure 5, when hematite is fractured along the basal plane, the longer Fe-O bonds would break so that on average every other Fe atom—one from each pair—would ideally go to each of the two surfaces created by fracture along parting (Kurtz and Henrich, 1983). If this is the case, then only half the Fe atoms of an Fe layer in bulk hematite survive on a given {001} surface, most likely those that are not face-sharing octahedra with the next layer down. These surface Fe atoms would immediately repopulate their first coordination shells with O or H_2O molecules adsorbed from the air. In the absence of significant lateral relaxation or reconstruction, these Fe atoms would be expected to maintain their 5-Å distances as in the original bulk structure. Hochella et al. (1989) demonstrated with LEED that the {001} surface of hematite fractured along parting under air has surface unit-cell dimensions of 5.07 Å—within error for surface electron diffraction of the bulk unit-cell dimensions (5.04 Å)—and that the surface structure was probably not reconstructed in the plane of fracture.

The symmetry and separation of peaks in Figure 4A therefore are entirely consistent with the anticipated surface configuration of hematite and with the surface unit-cell dimension of 5.07 Å determined by LEED (Hochella et al., 1989). This image also shows a marked similarity to atomic-scale STM images of the Fe array on the hematite {001} surface. Figure 4B, which was produced by

STM using a +1100 mV sample bias voltage, shows a hexagonal array of peaks with ~5-Å nearest neighbor separation, which probably corresponds to states localized on Fe sites. Peak heights are ~0.2–0.3 Å. Images produced by Eggleston et al. (1990) using a −300 mV sample bias voltage (not shown here) showed the O array on the {001} surface of hematite with hexagonal symmetry and 2.9-Å spacing. Comparison of the AFM image with the STM and LEED data therefore suggests that the peaks on the AFM image correspond to the surface Fe array, probably with attached coordinating (O, OH, H_2O) sorbates.

Conclusions

The AFM images presented in this paper depict nanometer- and molecular-scale structures imaged on the surface of a geologically important mineral phase in situ. Images of surface structures under H_2O suggest that AFM will be a valuable tool for studying processes at the mineral-H_2O interface. Comparison of AFM and STM images in air demonstrates that these two scanning probe microscopes, which rely on very different physical operating mechanisms (atom-atom repulsion vs. electron tunneling), can produce remarkably similar high-resolution images. For semiconducting minerals such as hematite, the two techniques thus may provide complementary capabilities, allowing us to study surface structure, chemical composition, and chemical reactivity in situ. In combination with classical geochemical techniques, with surface sensitive spectroscopies, and with continued advances in image interpretation, AFM and STM promise to open new and previously unexplored avenues of research in geochemistry.

Acknowledgments

We thank George A. Parks, Frederick J. Wicks, and an anonymous reviewer for valuable review comments. Virgil Elings and Kevin Kjoller of Digital Instruments generously shared their expertise on AFM use in numerous conversations with our group, and their help is greatly appreciated. We are indebted to the Center for Materials Research and the McGee Fund at Stanford University, to NSF graduate fellowships, and also to the Petroleum Research Fund of the American Chemical Society (no. 22892-AC5,2 to M.F.H.) for supporting this work.

References cited

Albrecht, T.R., and Quate, C.F. (1988) Atomic resolution with the atomic force microscope on conductors and non-conductors. Journal of Vacuum Science Technology, A6, 271–274.

Binnig, G., Quate, C.F., and Gerber, Ch. (1986) Atomic force microscope. Physical Review Letters, 56, 930–933.

Blake, R.L., Hessevick, R.E., Zoltai, T., and Finger, L.W. (1966) Refinement of the hematite structure. American Mineralogist, 51, 123–128.

Eggleston, C.M., and Hochella, M.F., Jr. (1990) Scanning tunneling microscopy and spectroscopy of sulfide surfaces. Geochimica et Cosmochimica Acta, 54, 1511–1519.

Eggleston, C.M., Hochella, M.F., Jr., and Parks, G.A. (1990) Surface structure of hematite (001) by scanning tunneling microscopy: Direct observation of surface relaxation. Geological Society of America Abstracts with Programs, A292.

Hartman, H., Sposito, G., Yang, A., Manne, S., Gould, S.A.C., and Hansma, P.K. (1990) Molecular-scale imaging of clay mineral surfaces with the atomic force microscope. Clays and Clay Minerals, 38, 337–342.

Hochella, M.F., Jr. (1990) Atomic structure, microtopography, composition, and reactivity of mineral surfaces. In Mineralogical Society of America Reviews in Mineralogy, 23, 87–132.

Hochella, M.F., Jr., Eggleston, C.M., Elings, V.B., Parks, G.A., Brown, G.E., Jr., Wu, C.M., and Kjoller, K. (1989) Mineralogy in two dimensions: Scanning tunneling microscopy of semiconducting minerals with implications for geochemical reactivity. American Mineralogist, 74, 1233–1246.

Hochella, M.F., Jr., Eggleston, C.M., Elings, V.B., and Thompson, M.S. (1990) Atomic structure and morphology of the albite (010) surface: An atomic-force microscope and electron diffraction study. American Mineralogist, 75, 723–730.

Kurtz, R.L., and Henrich, V.E. (1983) Geometric structure of the α-Fe_2O_3 (001) surface: A LEED and XPS study. Surface Science, 129, 345–354.

Meyer, G., and Amer, N.M. (1990) Optical-beam deflection atomic force microscopy: The NaCl (001) surface. Applied Physics Letters, 56, 2100–2101.

Sharp, T. G., Zheng, Nan Jiu, Tsong, I.S.T., and Buseck, P.R. (1990) Scanning tunneling microscopy of defects in Ag- and Sb-bearing galena. American Mineralogist, 75, 1438–1442.

Weisenhorn, A.L., Mac Dougall, J.E., Gould, S.A.C., Cox, S.D., Wise, W.S., Massie, J., Maivald, P., Elings, V.B., Stucky, G.D., and Hansma, P.K. (1990) Imaging and manipulating molecules on a zeolite surface with the atomic force microscope. Science, 247, 1330–1333.

Manuscript received March 6, 1991
Manuscript accepted May 2, 1991